

# Nonlinear Dynamics of Bubbles in Tissue

---

David Sinden  
Fraunhofer Institute for Digital Medicine MEVIS  
Dynamical Systems Seminar

January 23<sup>th</sup> 2024

University of Bremen

## Outline

---

Therapeutic Ultrasound

Bubble Dynamics & Inertial Collapse

Bifurcation Type

Bubble-Bubble Interactions

Koopman Operators and Control

Pulsed Doppler Imaging

Conclusions

## Therapeutic Ultrasound

---

High-intensity focused ultrasound is

- Non-ionizing – no harmful side effects, can be performed many times without accumulating dose
- Non-invasive – no cutting, so reduced risk of infection, shorter recovery time
- Selectively target regions within patient – can target regions surrounded by sensitive structures, can be used in some hard to access regions, and spares healthy tissue
- In many case, can be monitored in real time, so can see the correct dose is being delivered to the correct location

Main mechanisms of therapeutic action:

### Thermal

Heating tissue through absorption of the acoustic energy [1]. Approved for clinical use and reimbursement in a number of cases.

and

### Mechanical

Rupturing tissue through either acoustic wave or through bubble nucleation and collapse (histotripsy) [2].

Subsequently,

### Immune

There is increasing evidence that the thermal and mechanical effects of ultrasound can stimulate an immune response [3].

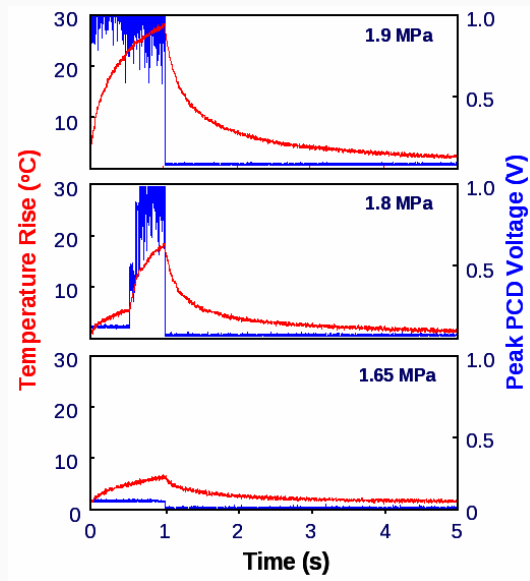


**Figure 1:** As the strength of the applied ultrasound field increases, cavitation is detected. Cavitation activity, in blue, is correlated with increased heating, in red, [4].

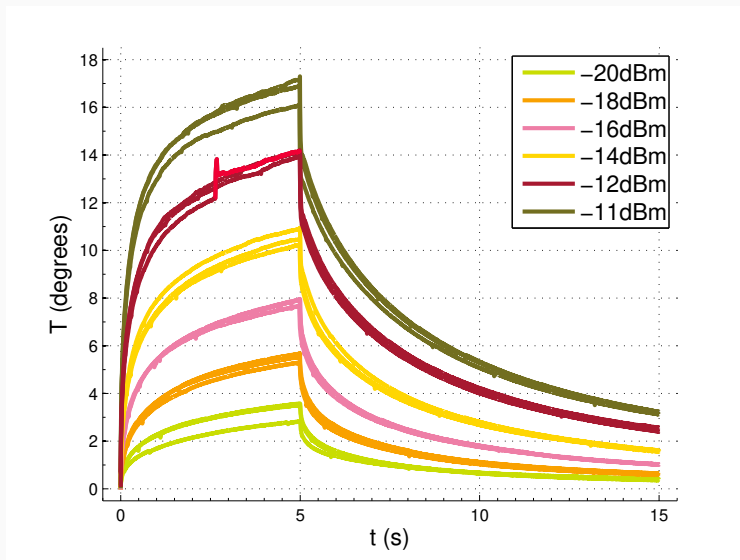


Figure 2: Isolated instance of cavitation activity near the temperature measurement device



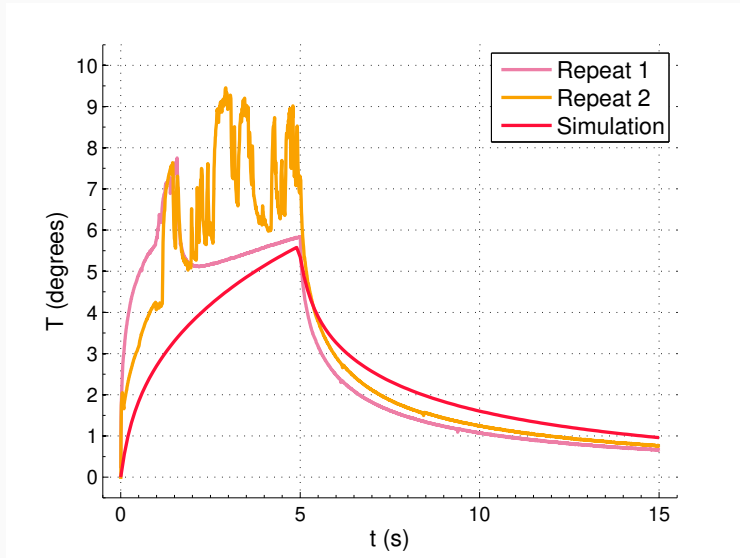


Figure 3: Sustained cavitation activity near the temperature measurement device

Bubble oscillations were one of the very first examples of nonlinear dynamical system, dates back to a publication from 1976 [5]

## **Numerical investigation of nonlinear oscillations of gas bubbles in liquids\***

Werner Lauterborn

*Drittes Physikalisches Institut, Universität Göttingen, D-34 Göttingen, West Germany*  
(Received 28 December 1973; revised 27 August 1974)

Forced oscillations of a spherical gas bubble in an incompressible, viscous liquid (water) are calculated numerically. The information gathered is mainly displayed in the form of frequency response curves of the steady-state solutions showing the harmonics, subharmonics, and ultraharmonics. Bubbles oscillating ultraharmonically at frequencies below the main resonance may emit half the driving frequency. This fact gives rise to a new explanation for the occurrence of the first subharmonic in the spectrum of the cavitation noise in ultrasonic cavitation.

Subject Classification: [43]30.70, [43]30.75.

Governing equation for the change in the radius of a bubble, driven by an external acoustic field, is given by the second-order nonlinear ordinary differential equation

$$\begin{aligned}
 \rho \left( \ddot{R}R + \frac{3}{2} \dot{R}^2 \right) = & p_g(R) + p_v - p(t) - \frac{2\sigma}{R} - \frac{4\mu\dot{R}}{R} \\
 & + \int_a^b \frac{\tau_{rr}}{r} ds + \frac{R}{c} \frac{d}{dt} (p_g - p) .
 \end{aligned} \tag{1}$$

The equation is annotated with the following terms and their physical meanings:

- $\rho$ : density
- $p_g(R)$ : (internal) gas pressure
- $p_v$ : vapour pressure
- $p(t)$ : external pressure
- $\frac{2\sigma}{R}$ : surface tension
- $\frac{4\mu\dot{R}}{R}$ : viscosity
- $\int_a^b \frac{\tau_{rr}}{r} ds$ : rheological effects
- $\frac{R}{c} \frac{d}{dt} (p_g - p)$ : 2<sup>nd</sup> order correction,  $c$  is speed of sound

Typically rheological effects are ignored, as at scales considered, tissue behaves like a fluid to the bubble.

The governing equation can accurately predict bubbles dynamics.

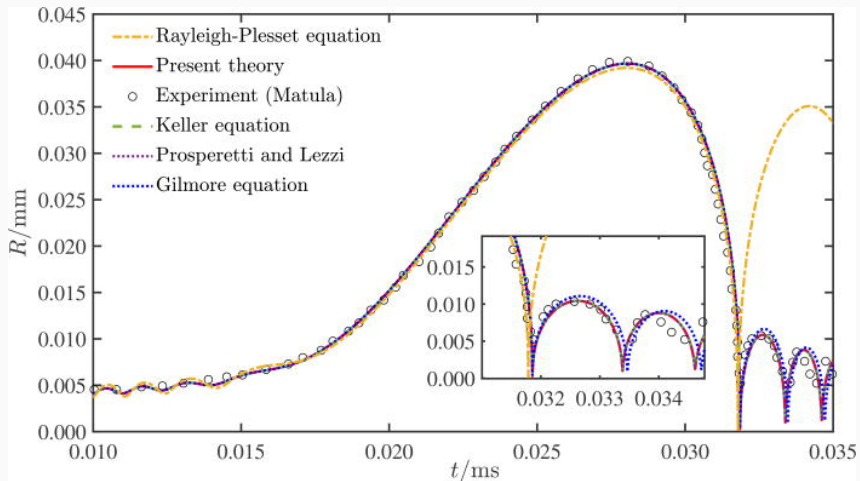


Figure 4: From [6, 7]

## Bubble Dynamics & Inertial Collapse

---

With increasing pressure, the bubble oscillates in a nonlinear manner. This is interpreted to mean that the oscillations from a sinusoidal applied field are not well approximated by a linear oscillator.

Note that the bubble collapse occurs during the rarefaction phase of the applied acoustic wave.

The bubble expands too much and can not support itself and collapses.

Such a collapse is said to be inertially driven, and referred to as inertial cavitation

**Inertial cavitation** typically occurs when the maximum radius is more than twice the initial radius.

Cavitation can be either stable or transient, and either inertial or non-inertial. Most measurements of cavitation activity are either stable non-inertial or transient inertial cavitation. Inertial cavitation is often assumed to be chaotic (and transient).

The stable, non-inertial oscillations can be used to open the blood-brain-barrier and deliver drugs to the brain [8].

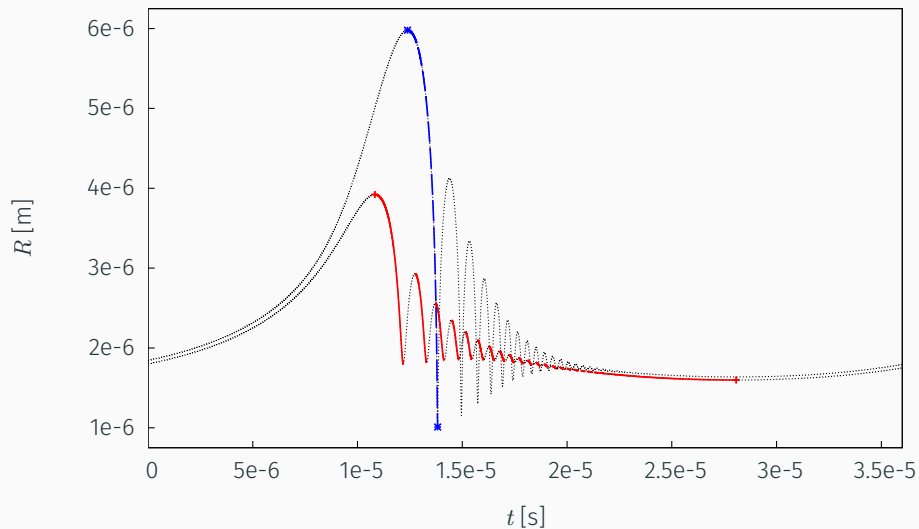


**Figure 5:** Inertial cavitation is characterised by a sudden change in the expansion of the bubble and rapid collapse if the initial radius of the bubble changes slightly. Only for inertial cavitation is enhanced heating observed.



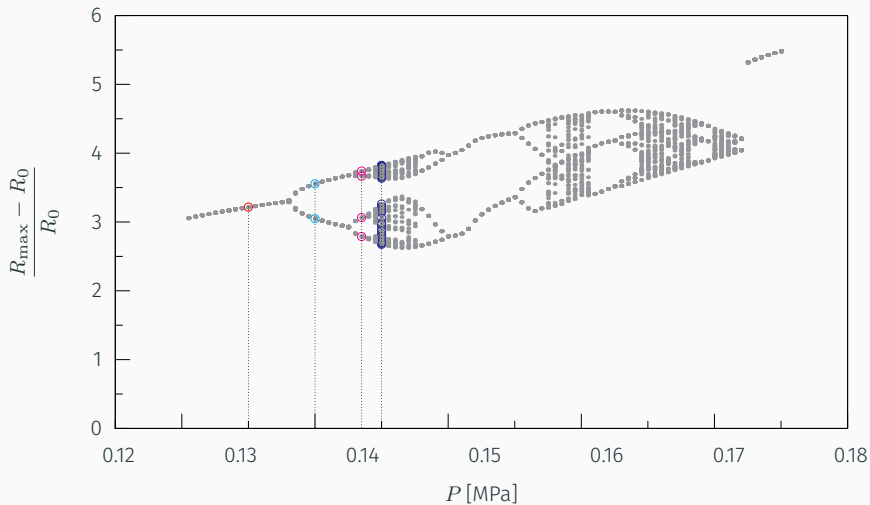


**Figure 6:** Bifurcation diagram for  $R_0 = 1.4 \mu\text{m}$ : one-period at  $P = 0.13$  MPa, two-period at  $0.135$  MPa, four-period at  $0.1375$  MPa and quasi-periodic at  $0.14$  MPa.

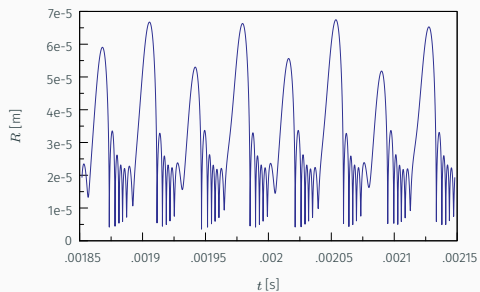
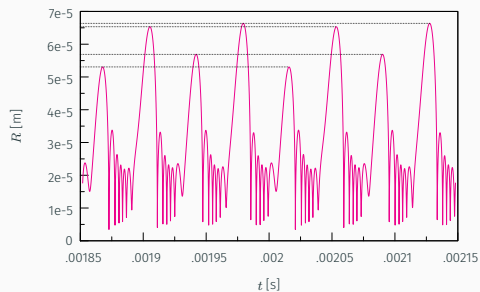
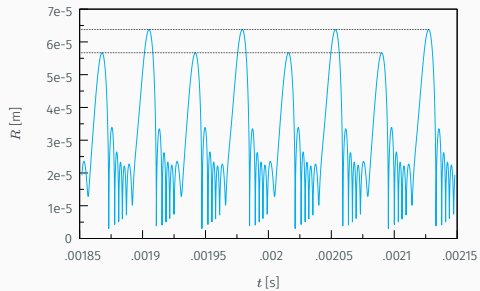
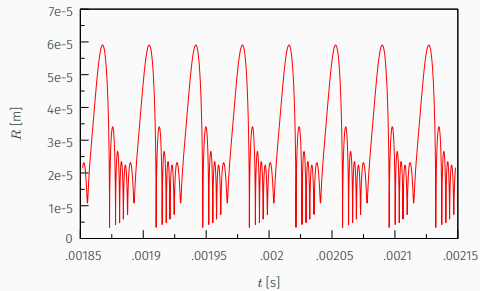


**Figure 7:** Radius-time curves beyond show period-doubling cascade to chaos.

The thresholds for unpredictable oscillations, which are associated with large oscillation, inertial collapse, and increase heat deposition can be investigated. The resonant frequency of the system is given by

$$\omega^* = \sqrt{\frac{4\sigma}{\rho R_0^3} + \frac{3(p_0^\infty - p_v)}{\rho R_0^2}}$$

where  $p_0^\infty$  is the ambient pressure. The Blake critical radius is given by

$$R_c = R_0 \sqrt{\frac{3R_0}{2\sigma} + \left(p_0^\infty - p_v + \frac{2\sigma}{R_0}\right)}.$$

Investigate the dynamics in the neighbourhood of the critical radius. Let  $\varepsilon = 2(1 - R_0/R_c)$  and set  $R = R_0(1 - \varepsilon x)$  and scale  $\tau = \omega^* t$ , so that

$$\omega^* = \sqrt{\frac{2\sigma\varepsilon}{\rho R_0^3}}.$$

At  $\mathcal{O}(\varepsilon^2)$ , the Rayleigh–Plesset equation (1) then has the normal form [9]

$$\ddot{x} + 2\zeta\dot{x} + x(1-x) = A \sin(\Omega\tau)$$

where  $\zeta$ ,  $A$  and  $\Omega$  are all  $\mathcal{O}(1)$  for typical parameters. In the absence of forcing, the system has a centre at  $(0, 0)$  and saddle point at  $(1, 0)$ . There is a homoclinic orbit to the unperturbed saddle, given by

$$x = \frac{1}{2} \left( \tanh^2(\tau/2) - 1 \right).$$

Perform Mel'nikov analysis when the applied acoustic field is considered to be small, yielding a relationship for chaotic oscillations (sensitivity to initial conditions) in the vicinity of the critical point, and yields a lower bound for transverse intersection of stable and unstable manifolds of the perturbed saddle point

$$A = \frac{2\zeta \sinh(\pi\Omega^*)}{5\pi(\Omega^*)^2}.$$

For nonlinear wave propagation, the bound changes as the forcing term can be expressed as sum of higher frequency components [10].

**Integrated broadband noise** is defined by taking the Fourier transform of the measured acoustic signal from bubble activity over a short time period, removing the fundamental and harmonics of the signal, and integrating the remaining frequency content<sup>1</sup>.

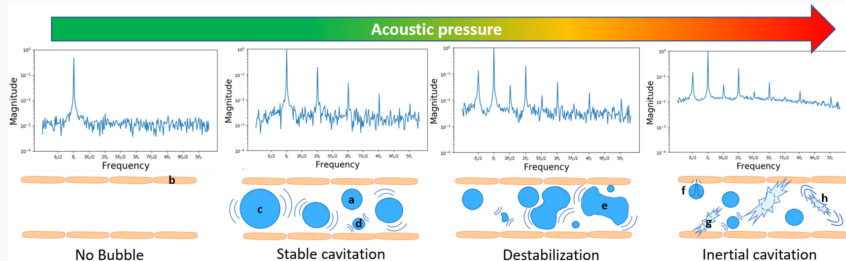


Figure 8: Spectra of non-inertial and inertial cavitation [11]

<sup>1</sup>Indeed, the appearance of noise was initially used to characterise chaotic oscillations [5]

If the noise is significantly above the typical baseline, then this is an indicator of inertial cavitation, and is correlated with the bioeffects associated with bubble activity.

### Research Question

Can it be proved, that high values of integrated broadband noise, i.e. a dense frequency spectrum, or area in Poincaré section / stroboscopic map, imply inertial cavitation?

## Bifurcation Type

---

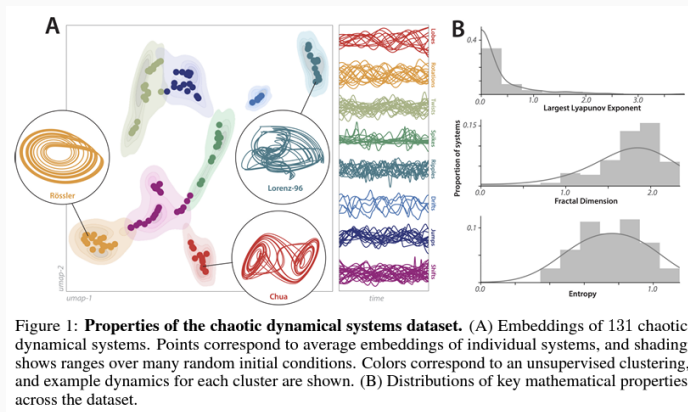
Bifurcation diagrams show, at kilohertz frequencies, and above, a subharmonic, period-doubling route to chaos [12].

De la Rosa [13] presented bifurcation diagrams which suggested that at far lower ultrasonic frequencies driving frequencies, oscillations were more like intermittency route to chaos from a saddle-node bifurcation.



# Period Doubling and Intermittency

Can the path of the attractor be traced through a parameter space at the critical pressures for a given frequency at which chaos is observed, and compute quantitative differences, as per Gilpin [14] between 70 kHz and 500 kHz.



Interaction

---



It has been conjectured, based on delay embedding reconstructions of the phase space from experimentally observed data, that phase synchronisation occurs with a **bubble cloud** as the reconstructed attractor has an embedding dimension slightly greater than two [16, 17, 18], whereas the number of degrees of freedom of the governing equations would be exceptionally large.

Furthermore, the received signal from an oscillating cloud of bubbles contains a subharmonic component of magnitude which can not be derived from models where a collection of single bubbles with differing radii oscillate independently.

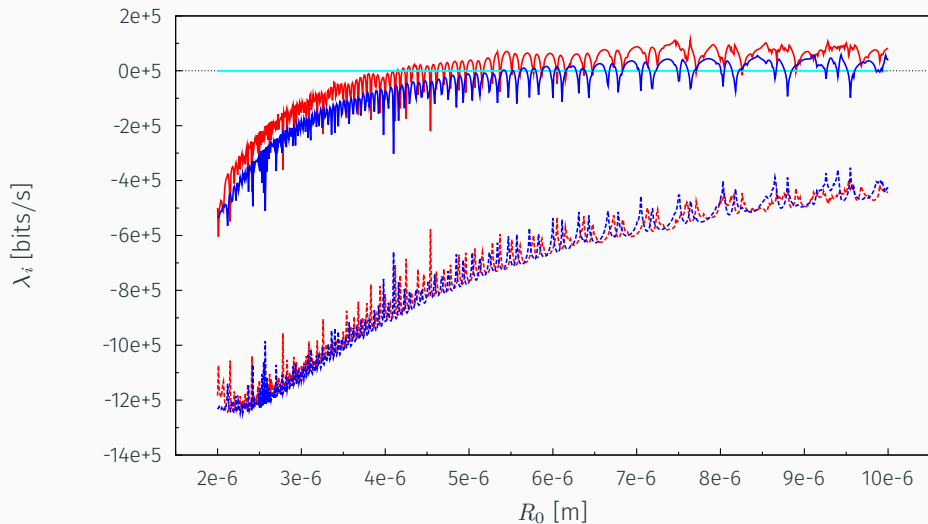


Figure 9: Lyapunov exponent of pair of bubbles, at distance of  $100 \mu\text{m}$ .

A single positive Lyapunov exponent suggests that one bubble is oscillating in an unpredictable manner, hence the reradiated field is also chaotic. This field, combined with the applied field, then drives the other bubble in a deterministic manner.

The existence of two positive Lyapunov exponents suggests that each bubble is oscillating in a chaotic manner.

### Question

Are there parameter regimes in which each bubble, without interaction, would oscillate in a regular manner, but with interaction has a two positive Lyapunov exponents?

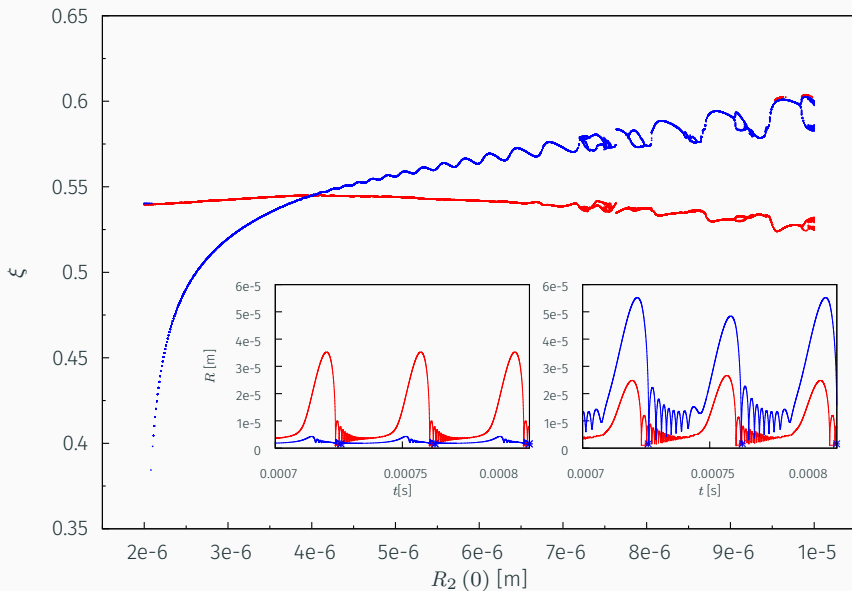


**Figure 10:** Bifurcation diagram for coupled bubble pair as initial radius  $R_2$  is varied, showing when the time of collapse within an acoustic cycle.

Control

---



Can the behaviour of the bubbles be controlled?

As seen, the state space is complicated.

Koopman operator theory seeks to transform **nonlinear** dynamics from state space to **linear** dynamics in Koopman-invariant function space.

$$\dot{\mathbf{x}} = f(\mathbf{x}) \mapsto \dot{g} = \mathcal{K}g$$

The formulation as a linear system allows for classical, realisable, control strategies to be derived and employed. Two main control functions are the linear-quadratic regulator (LQR) and the model-predictive control (PMC).

The Koopman operator,  $\mathcal{K}$ , is infinite-dimensional, acts on observable,  $g(\mathbf{x}) : \mathcal{M} \rightarrow \mathbb{R}$ .

Apply spectral theory,

$$\dot{\varphi}_k(\mathbf{x}) = \mathcal{K}\varphi_k(\mathbf{x}) = \lambda_k\varphi_k(\mathbf{x})$$

for eigenfunctions  $\varphi_k$  of the operator. So that

$$g(\mathbf{x}) \approx \sum_{k=1}^n v_k \varphi_k(\mathbf{x})$$

for  $n$  complex eigenfunctions [19, 20], where the Koopman operator is defined as

$$\mathcal{K}^{t_0} g(\mathbf{x}) = g(\mathbf{x}(t + t_0)) \quad \Rightarrow \quad \mathcal{K}g = \lim_{t_0 \rightarrow 0} \frac{\mathcal{K}^{t_0} g - g}{t_0}.$$

Gibson, Yee and Calvisi [21] approximated the

- Koopman eigenfunctions using sparse identification of nonlinear dynamical systems (SINDy) [22] with fourth-order polynomials

and used

- Hankel dynamic mode decomposition (HDMD) [19] to compute the complex eigenvalues.

The training data used to approximate the Koopman operator was the oscillation of a single simulated bubble modelled by the Rayleigh-Plesset equation (1) without forcing.

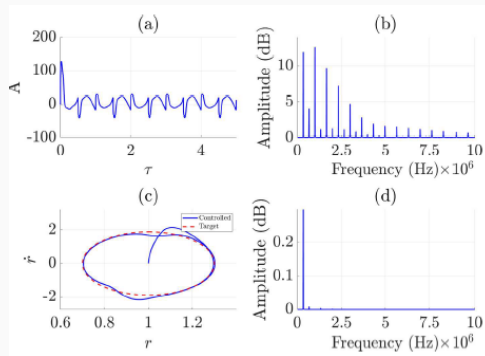
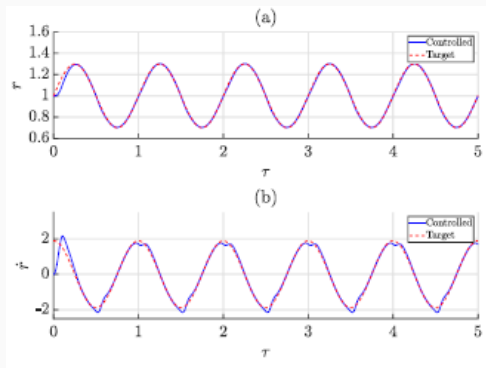
The initial radius of the bubble was set to 37% of its equilibrium value so that the bubble expands (reaching close to twice its equilibrium radius) and the resulting oscillations are nonlinear.

Gibson, Yee and Calvisi [21] construct a cost function of the form

$$J_{\Omega} = \frac{1}{2} \int_0^{\infty} \left( Q^T R Q + u^T R u \right) dt$$

where  $u$  is the control forcing term,  $\Omega$  is the matrix comprised on the real and imaginary parts of the Koopman eigenfunctions, and  $Q = \mathcal{Q}I$ ,  $R = \mathcal{R}I$ , where  $\mathcal{Q}$  and  $\mathcal{R}$  are scalar tuning parameters.

Solved subject to a constraint on the evolution, yielding a state-dependent algebraic Riccati equation.



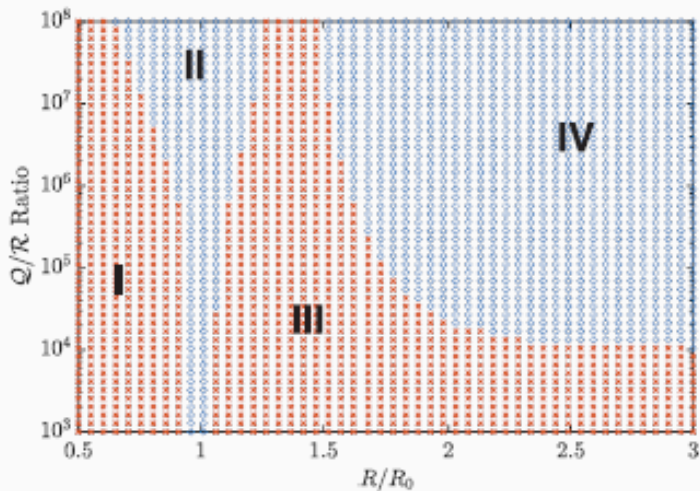


Figure 11: Red regions are those which fail to stabilize a bubble to a target radius, from [21, Fig 16].

## Pulsed Doppler Imaging

---

It is desirable to be able to see bubbles caused by pulsed high-intensity focused ultrasound in tissue. These are a source of damage. These bubbles only exist for a up to a few hundred millisecond though.

Bubble Doppler sends an ultrasound pulse, then an sequence of planewave pulses which are used to reconstruct an image.

The fundamental idea of ultrasound imaging is to take a set of received time signals and, based on the amplitude of the envelope of the signals, form an image of the tissue properties.



However, extracting bubble dynamics from clutter and other phenomena requires a filter. Typically a singular value decomposition or infinite impulse response filter is used.

In the context of Doppler imaging these are referred to as wall filters as the aim was to remove motion of vessel wall from the

Recently dynamic mode decomposition was applied to separate the slow and fast time scales in time signal data [23, 24] which is used to reconstruct ultrasound images.

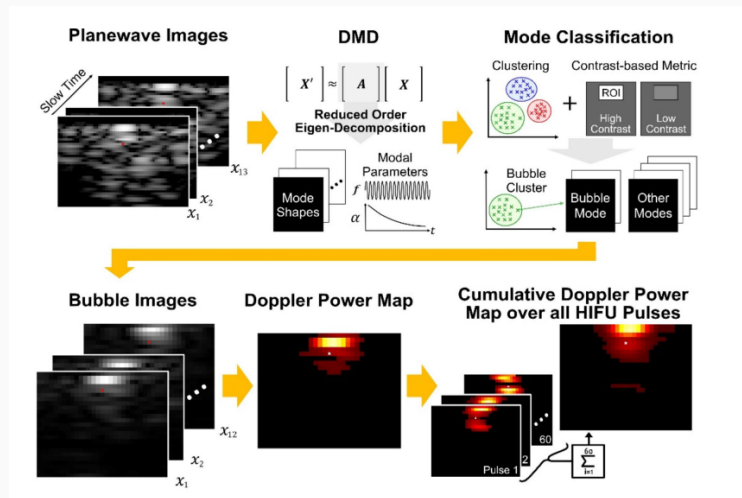


**Figure 12:** Schematic of pipeline from [24] showing spatial and temporal identification of transient bubble dynamics.

## Summary

---

- Clinical challenge is problem in **nonlinear dynamics**, with highly uncertain coefficients.
- Chaotic oscillations are likely to occur
- Broadband noise should be rigorously explained
  
- In bubble-bubble interactions attractor may exist in high dimensions – what are the consequences for bifurcations and received signal?
  
- Koopman operator theory has been employed to investigate control of bubbles [20, 21], but for single, free bubbles.





- Formal proof that broad noise is a result of chaotic oscillations of a single bubble, and that there are no other explanations.
  - Does the dimension of the attractor scale with the number of bubbles?
  - What other mechanisms produce broadband noise? What does broadband noise say about Poincaré sections
- Attractor reconstruction/continuation as driving frequency changes
- Construct Koopman operator for
  - multiple bubbles, firstly of pair of equally size interacting bubbles
  - populations of mono-disperse encapsulated microbubbles
  - Multiple target radius?
  - Derive a Koopman operator based on either simulated or measured observables, i.e. the re-radiated signal from a bubble, rather than radial oscillations

$$g(R) = R \left( R\ddot{R} + 2\dot{R}^2 \right)$$

could be propagated through material and averaged over the area of the sensor

# Thankyou for your attention

## Any questions?

  *david\_sinden*       *davidsinden.bsky.social*   
  *david.sinden@mevis.fraunhofer.de*   
  *github.com/djps/rayleigh-plesset*   
  *djps.github.io*

Creative Commons Attribution-ShareAlike 4.0 International License   

## References

---

- [1] J. E. Kennedy, G. R. ter Haar, and D. Cranston, “High intensity focused ultrasound: surgery of the future?” *Br. J. Radiol.*, vol. 76, no. 909, pp. 590–599, 2003.
- [2] M. A. O’Reilly, “Exploiting the mechanical effects of ultrasound for noninvasive therapy,” *Science*, vol. 385, no. 6714, p. eadp7206, 2024.
- [3] J. Unga and M. Hashida, “Ultrasound induced cancer immunotherapy,” *Adv. Drug Deliv. Rev.*, vol. 72, pp. 144–153, 2014.
- [4] C. C. Coussios, C. H. Farny, G. Ter Haar, and R. A. Roy, “Role of acoustic cavitation in the delivery and monitoring of cancer treatment by high-intensity focused ultrasound (HIFU),” *Int. J. Hyperthermia*, vol. 23, no. 2, pp. 105–120, 2007.
- [5] W. Lauterborn, “Numerical investigation of nonlinear oscillations of gas bubbles in liquids,” *J. Acoust. Soc. Am.*, vol. 59, no. 2, pp. 283–293, 1976.
- [6] A. Zhang, S.-M. Li, P. Cui, S. Li, and Y.-L. Liu, “A unified theory for bubble dynamics,” *Phys. Fluids*, vol. 35, no. 3, 2023.



- [7] T. J. Matula, “Inertial cavitation and single-bubble sonoluminescence,” *Phil. Trans. R. Soc. Lond. A*, vol. 357, no. 1751, pp. 225–249, 1999.
- [8] T. Sun, G. Samiotaki, S. Wang, C. Acosta, C. C. Chen, and E. E. Konofagou, “Acoustic cavitation-based monitoring of the reversibility and permeability of ultrasound-induced blood-brain barrier opening,” *Phys. Med. Biol.*, vol. 60, no. 23, p. 9079, 2015.
- [9] A. Harkin, A. Nadim, and T. J. Kaper, “On acoustic cavitation of slightly subcritical bubbles,” *Phys. Fluids*, vol. 11, no. 2, pp. 274–287, 1999.
- [10] D. Sinden, E. Stride, and N. Saffari, “The effects of nonlinear wave propagation on the stability of inertial cavitation,” in *J. Phys. Conf. Ser.*, vol. 195, no. 1. IOP Publishing, 2009, p. 012008.
- [11] P. Mondou, S. Mériaux, F. Nageotte, J. Vappou, A. Novell, and B. Larrat, “State of the art on microbubble cavitation monitoring and feedback control for blood-brain-barrier opening using focused ultrasound,” *Phys. Med. Biol.*, vol. 68, no. 18, p. 18TR03, 2023.
- [12] W. Lauterborn and U. Parlitz, “Methods of chaos physics and their application to acoustics,” *J. Acoust. Soc. Am.*, vol. 84, no. 6, pp. 1975–1993, 1988.

- [13] M. A. D. de la Rosa, G. A. Hussein, and W. G. Pitt, “Comparing microbubble cavitation at 500 kHz and 70 kHz related to micellar drug delivery using ultrasound,” *Ultrasonics*, vol. 53, no. 2, pp. 377–386, 2013.
- [14] W. Gilpin, “Chaos as an interpretable benchmark for forecasting and data-driven modelling,” *arXiv preprint arXiv:2110.05266*, 2021.
- [15] O. E. Rossler, “An equation for hyperchaos,” *Phys. Letts A*, vol. 71, no. 2-3, pp. 155–157, 1979.
- [16] W. Lauterborn and J. Holzfuss, “Evidence for a low-dimensional strange attractor in acoustic turbulence,” *Phys. Letts. A*, vol. 115, no. 8, pp. 369–372, 1986.
- [17] S. Luther, M. Sushchik, U. Parlitz, I. Akhatov, and W. Lauterborn, “Is cavitation noise governed by a low-dimensional chaotic attractor?” in *Nonlinear acoustics at the turn of the millennium*, ser. Am. Inst. Phys. Conf. Ser., W. Lauterborn and T. Kurz, Eds., vol. 524. Melville, NY: Am. Inst. Phys., 2000, pp. 355–358.
- [18] J. Holzfuss and W. Lauterborn, “Liapunov exponents from a time series of acoustic chaos,” *Phys. Rev. A*, vol. 39, no. 4, pp. 2146–2152, 1989.

- [19] H. Arbabi and I. Mezic, “Ergodic theory, dynamic mode decomposition, and computation of spectral properties of the Koopman operator,” *SIAM J. Appl. Dyn. Syst.*, vol. 16, no. 4, pp. 2096–2126, 2017.
- [20] A. J. Gibson, M. L. Calvisi, and X. C. Yee, “Koopman linear quadratic regulator using complex eigenfunctions for nonlinear dynamical systems,” *SIAM J. Appl. Dyn. Syst.*, vol. 21, no. 4, pp. 2463–2486, 2022.
- [21] A. J. Gibson, X. C. Yee, and M. L. Calvisi, “Data-driven acoustic control of a spherical bubble using a Koopman linear quadratic regulator,” *J. Acoust. Soc. Am.*, vol. 156, no. 1, pp. 229–243, 2024.
- [22] S. L. Brunton, J. L. Proctor, and J. N. Kutz, “Discovering governing equations from data by sparse identification of nonlinear dynamical systems,” *Proc. Nat. Acad. Sci.*, vol. 113, no. 15, pp. 3932–3937, 2016.
- [23] M. Song, O. A. Sapozhnikov, V. A. Khokhlova, and T. D. Khokhlova, “Dynamic mode decomposition for transient cavitation bubbles imaging in pulsed high intensity focused ultrasound therapy,” *IEEE Trans. Ultrason. Ferroelectr. Freq. Control.*, vol. 71, pp. 596–606, 2024.

- [24] M. Song, O. A. Sapozhnikov, V. A. Khokhlova, H. Son, S. Totten, Y.-N. Wang, and T. D. Khokhlova, “Dynamic mode decomposition based Doppler monitoring of de novo cavitation induced by pulsed HIFU: an in vivo feasibility study,” *Sci. Rep.*, vol. 14, no. 1, p. 22295, 2024.